# Electronic Supplementary Information

## New metal-anion radical framework materials: $Co^{II}$ compounds showing ferromagnetic to antiferromagnetic phase transition at about 344 K, and $Zn^{II}$ compounds exhibiting terminal anion ligand induced direct white-light-emission

**Guo-Ping Yong,* Ying-Zhou Li, Chong-Fu Li, Yi-Man Zhang and Wen-Long She**

Department of Chemistry, University of Science and Technology of China, Hefei 230026, P.R. China

E-mail: gpyong@ustc.edu.cn

**Table S1** Selected bond distances (Å) and angles (º) for compounds **1**, **2** and **4**[a]

| **1**[b] | | **2**[c] | | **4**[c] | |
|---|---|---|---|---|---|
| Zn(1)-O(1) | 1.944(3) | Zn(1)-O(1) | 1.946(2) | Co(1)-O(1) | 1.9271(15) |
| Zn(1)-O(2) | 1.966(4) | Zn(1)-O(2) | 1.962(2) | Co(1)-O(2) | 1.9561(14) |
| Zn(1)-N(1) | 2.008(4) | Zn(1)-N(1) | 2.015(2) | Co(1)-N(1) | 2.0197(18) |
| Zn(1)-N(3)#2 | 1.981(4) | Zn(1)-N(3)#2 | 1.979(2) | Co(1)-N(3)#2 | 2.0044(18) |
| C(14)-O(1) | 1.284(6) | C(14)-O(1) | 1.270(3) | C(14)-O(1) | 1.288(2) |
| O(1)-Zn(1)-O(2) | 99.42(19) | O(1)-Zn(1)-O(2) | 102.86(10) | O(1)-Co(1)-O(2) | 104.04(7) |
| O(1)-Zn(1)-N(1) | 96.24(16) | O(1)-Zn(1)-N(1) | 96.45(9) | O(1)-Co(1)-N(1) | 96.45(7) |
| O(1)-Zn(1)-N(3)#2 | 108.39(16) | O(1)-Zn(1)-N(3)#2 | 107.53(9) | O(1)-Co(1)-N(3)#2 | 108.85(7) |
| O(2)-Zn(1)-N(1) | 113.96(19) | O(2)-Zn(1)-N(1) | 116.21(10) | O(2)-Co(1)-N(1) | 119.28(7) |
| O(2)-Zn(1)-N(3)#2 | 115.06(19) | O(2)-Zn(1)-N(3)#2 | 110.61(10) | O(2)-Co(1)-N(3)#2 | 110.62(7) |
| N(1)-Zn(1)-N(3)#2 | 119.45(17) | N(1)-Zn(1)-N(3)#2 | 120.11(10) | N(1)-Co(1)-N(3)#2 | 115.39(8) |

[a] According that data/crystal quality of **3** is not good, it is only given as a partial determination, the bond distances and angles of compound **3** are not provided.
[b] Symmetry code for compound **1**: #2 = *-x+1/2, y+1/2, -z+1/2*.
[c] Symmetry code for compounds **2** and **4**: #2 = *-x, y+1/2, -z+1/2*.

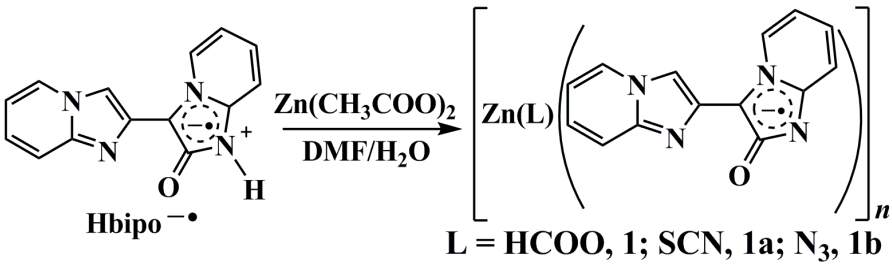


**Scheme S1** Synthesis of isomorphous zinc-anion radical frameworks from zwitterionic radical.

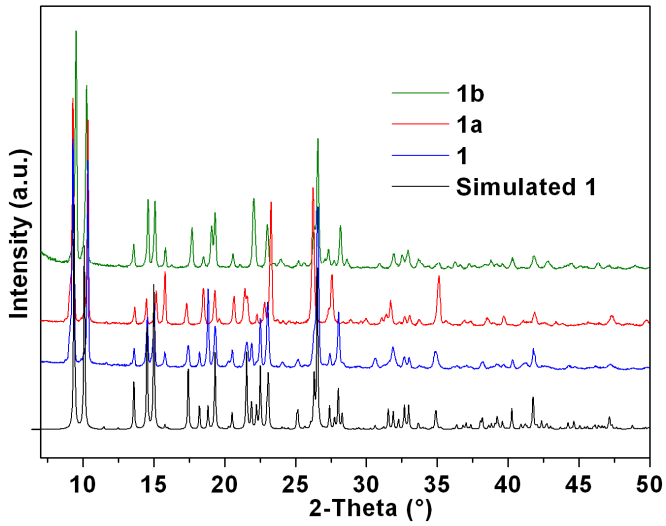


**Fig. S1** PXRD patterns of simulated **1** from the X-ray single-crystal structure, and synthesized **1**, **1a** and **1b**.

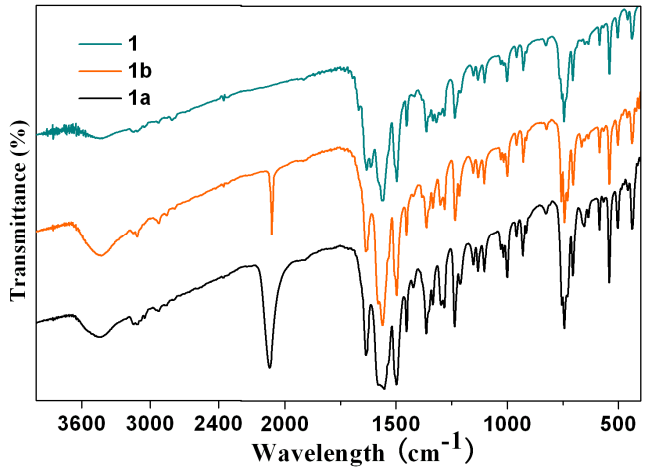


**Fig. S2** IR spectra of **1**, **1a** and **1b**, showing the characteristic band of the $SCN^-$ ligand at 2069 $cm^{-1}$ and $N_3^-$ ligand at 2059 $cm^{-1}$, respectively, attributed to the stretching vibration of the $SCN^-$ and $N_3^-$ group, respectively.

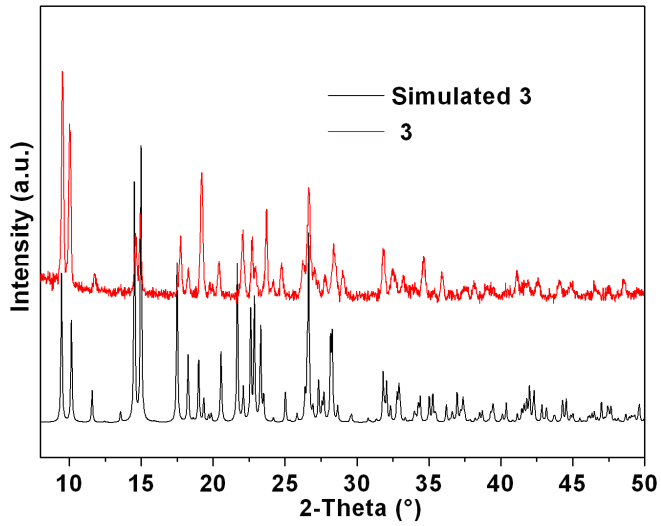


**Fig. S3** PXRD patterns of the simulated and synthesized **3**.

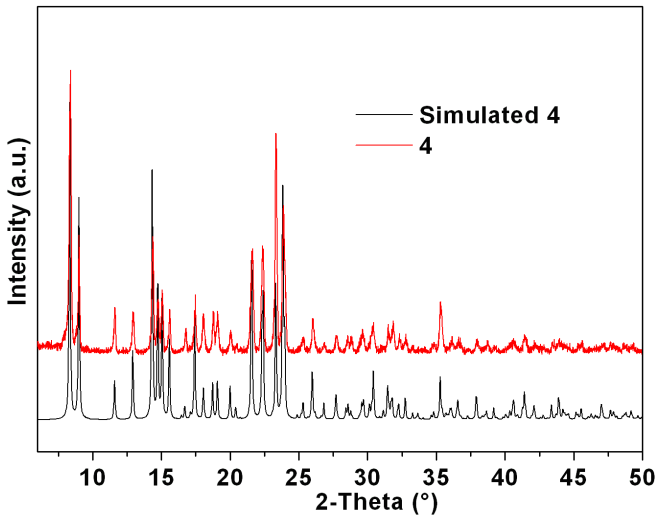


**Fig. S4** PXRD patterns of the simulated and synthesized **4**.

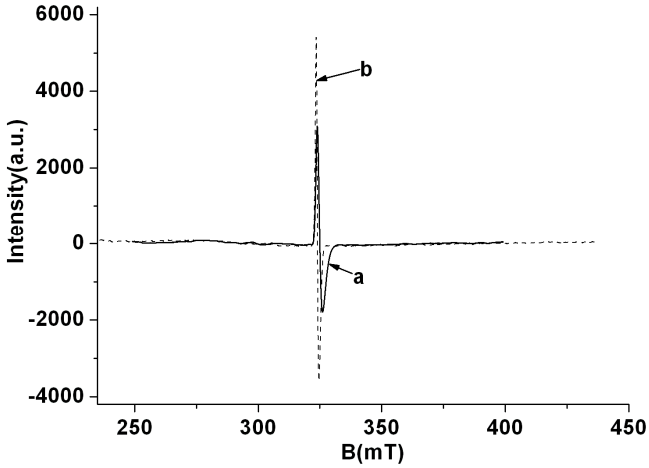


**Fig. S5** X-band EPR spectra of **1** (a) and **2** (b) at room temperature.

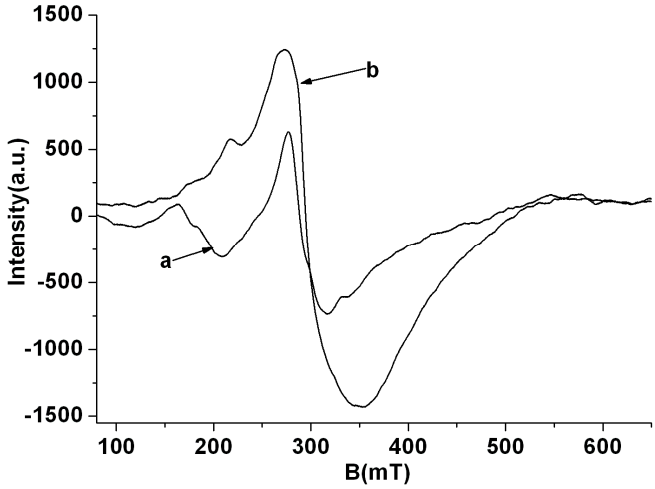


**Fig. S6** X-band EPR spectra of **3** (a) and **4** (b) at room temperature.

Noteworthy, except for one broad high field line (g = 2.240), compound **3** also shows another broad lower field satellite line (Fig. S6a), which probably arises from the magnetic field lying on different orientation of crystals of 1D chain structure.

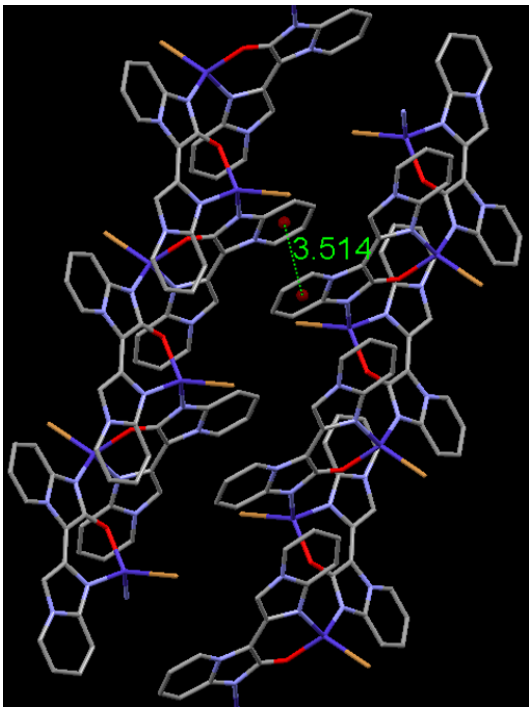


**Fig. S7** 2D network of **3** showing the π-π stacking interactions between adjacent chains.

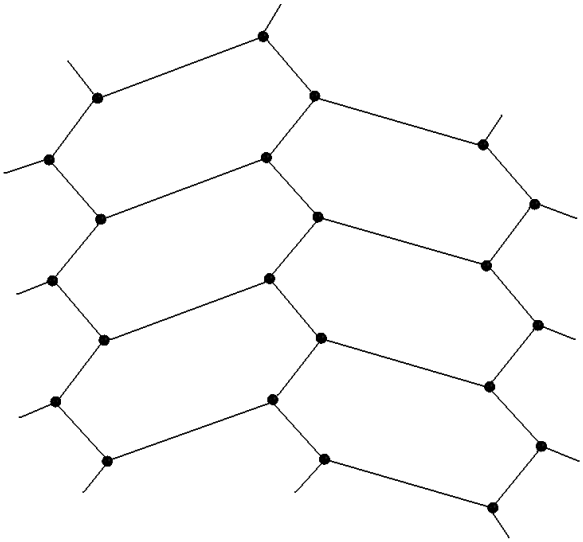

**Fig. S8** A topological illustration of the 2D (6, 3) network of compound **2**.

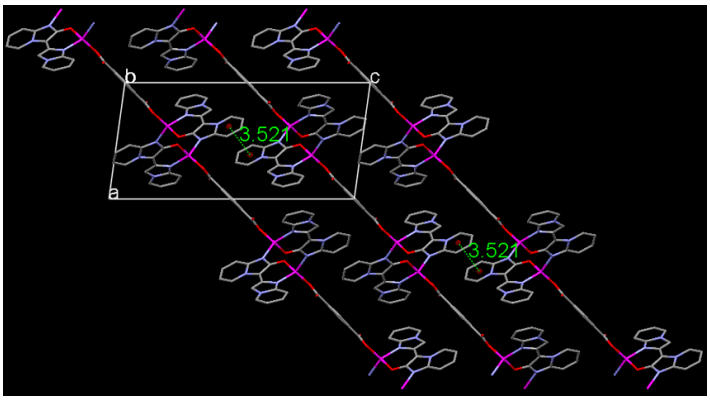


**Fig. S9** 3D framework of **2** as viewed down the *b*-axis, showing the offset π-π stacking interactions between 2D layers.

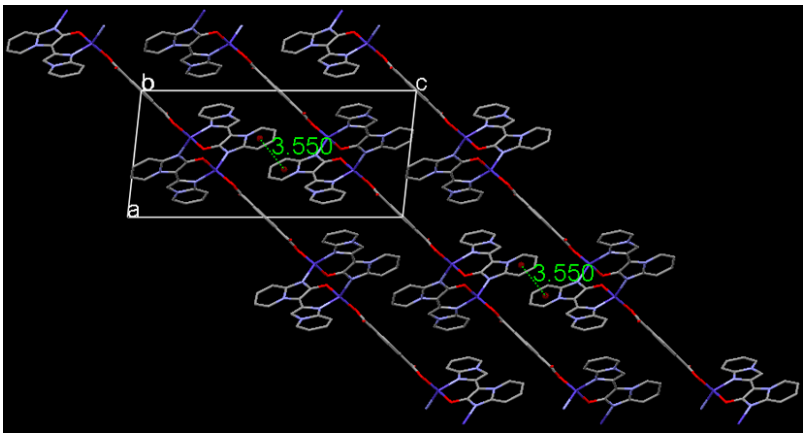


**Fig. S10** 3D framework of **4** as viewed down the *b*-axis, showing the offset π-π stacking interactions between 2D layers.

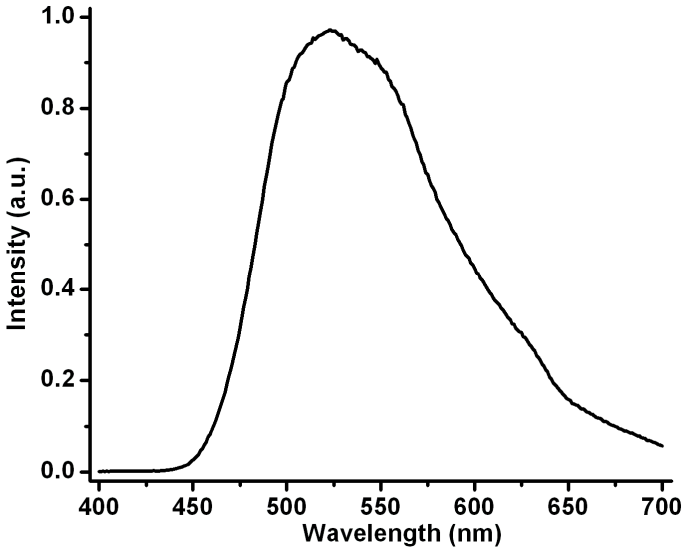


**Fig. S11** Solid photoluminescence spectrum of Hbipo$^{-\bullet}$ radical.

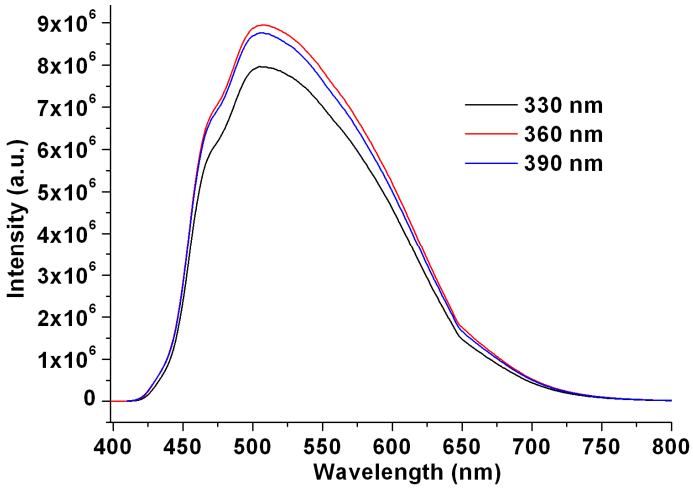


**Fig. S12** Solid state PL spectra of **1** by variation of excitation light under same metrical condition.

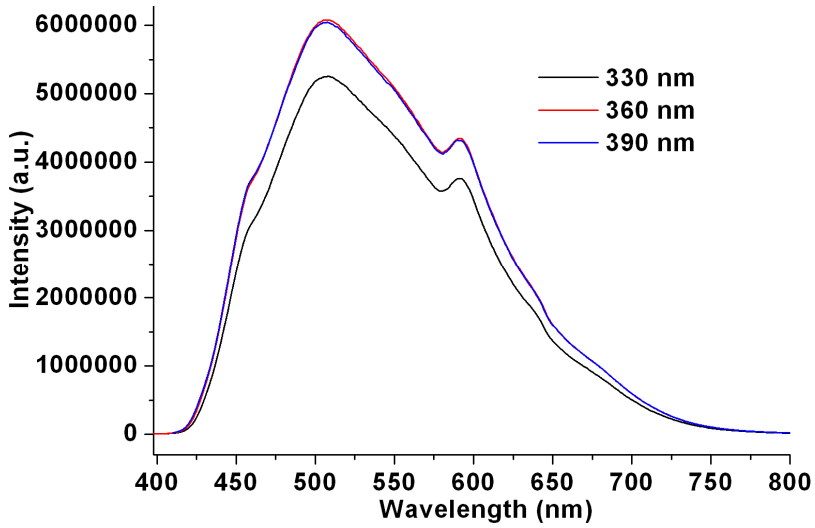


**Fig. S13** Solid state PL spectra of **1b** by variation of excitation light under same metrical condition.

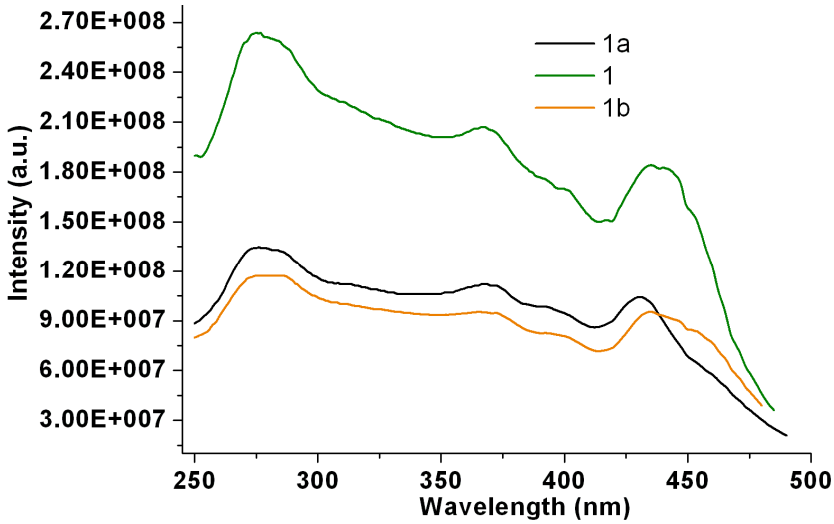


**Fig. S14** Solid excitation spectra of **1**, **1a** and **1b** at room temperature.

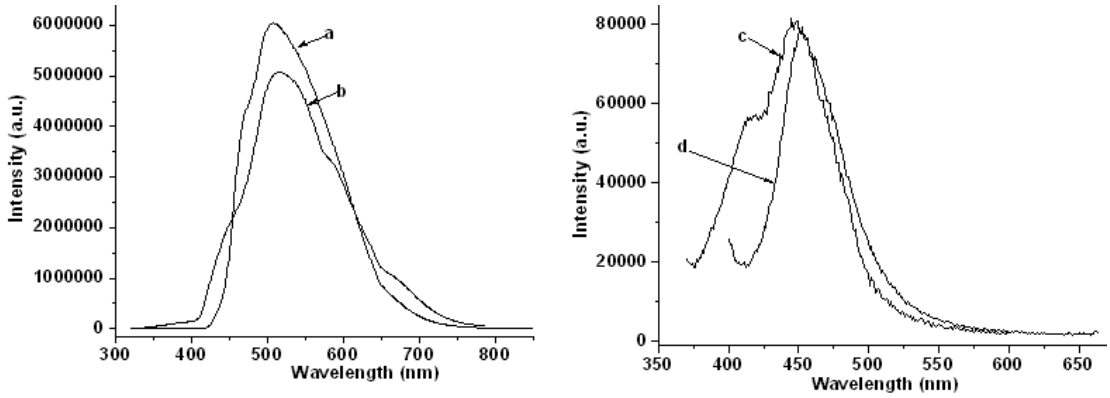


**Fig. S15** Solid PL spectra of compounds **1** (a), **2**(b), **3**(c) and **4**(d).